Balan, N., Zhang, Q.-H., Xing, Z., Skoug, R., Shiokawa, K., Lühr, H., Ram, S. T., Otsuka, Y., Zhao, L. (2019): Capability of Geomagnetic Storm Parameters to Identify Severe Space Weather. - The Astrophysical Journal, 887, 1, 51.

https://doi.org/10.3847/1538-4357/ab5113

Capability of Geomagnetic Storm Parameters to Identify Severe Space Weather

N. Balan[1,2], Qing-He Zhang[1], Zanyang Xing[1], R. Skoug[3], K. Shiokawa[4], H. Lühr[5], S. Tulasi Ram[6], Y. Otsuka[4], and Lingxin Zhao[1]

[1]Institute of Space Sciences, Shandong University, Weihai, Shandong 264209, China; [2]Institute of Geology and Geophysics, Chinese Academy of Sciences, Beijing 100029, China; [3]Los Alamos National Laboratory, Los Alamos, NM 87544, USA [4]Institute for Space-Earth Environmental Research, Nagoya University, Nagoya 464-8601, Japan [5]GFZ, German Research Centre for Geosciences, 14473 Potsdam, Germany. [6]Indian Institute of Geomagnetism, Navi Mumbai, 410218, India.

Correspondence to balan.nanan@yahoo.com

Running title: Severe space weather identification

Key words: Geomagnetic storm, IpsDst, severe space weather, solar wind and IMF

Abstract

The paper investigates the capability of geomagnetic storm parameters in Dst, Kp, and AE indices to distinguish between severe space weather (SvSW) causing the reported electric power outages and/or tele-communication failures and normal space weather (NSW) not causing such severe effects in a 50-year period (1958-2007). The parameters include the storm intensities DstMin (minimum Dst during the storm main phase MP), $(dDst/dt)_{MPmax}$, Kp_{max}, and $AE_{max.}$ In addition, the impulsive parameter IpsDst $= (-1/T_{MP})\int_{TMP}|Dst_{MP}|dt$ is derived for the storms automatically identified in Kyoto Dst and USGS Dst. $\int_{TMP}|Dst_{MP}|dt$ is the integral of the modulus of Dst from MP onset (MPO) to DstMin. T_{MP} is the MP duration from MPO to DstMin. The corresponding mean values $<Kp_{MP}>$ and $<AE_{MP}>$ are also calculated. Irrespective of the significant differences in the storm parameters between the two Dst indices, the IpsDst in both indices seems identifying 4 of the 5 SvSW events (and the Carrington event) from over 750 NSW events reported occurring in 1958-2007, while all other parameters separate 1 or 2 SvSW from NSW. Using a Kyoto IpsDst threshold of -250 nT, we demonstrate a 100% true SvSW identification rate with only one false NSW. Using the false NSW event (1972 August 04), we investigate whether using a higher-resolution Dst might result in a more accurate identification of SvSW. The mechanism of the impulsive action leading to large IpsDst and SvSW involves the coincidence of fast ICME velocity V containing its shock (or front) velocity $\triangle V$ and large IMF Bz southward covering $\triangle V$.

1. Introduction

A series of rapid changes takes place in interplanetary space (IPS) and the environment of planets during the passage of interplanetary coronal mass ejections (ICMEs) (e.g., Witasse et al. 2017), high-speed streams, and CIRs (co-rotating interaction regions) (Smith & Wolfe 1976). The changes are collectively called space weather. An ICME is a huge, magnetized (interplanetary magnetic field IMF up to 100 nT), high density (up to 100 cm^{-3}) plasma cloud ejected from the Sun and flowing out with speed up to thousands of km s^{-1} (e.g., Skoug et al. 2004). However, the part of the ICME that is most geoeffective is the magnetic cloud, which is a high magnetic field but low density region (Burlaga et al. 1981). A high speed ICME produces shock waves ahead, which accelerate the background charged particles to energies over 100 MeV, which are known as solar energetic particles or SEPs (e.g., Singh et al. 2010). The particles are accelerated to even higher energies by the high-speed ICME front that follows the ICME shock (e.g., Balan et al. 2014). They can damage satellite systems (e.g., Green et al. 2017) and are harmful for biological systems, for example, astronauts (e.g., Aran et al. 2005).

In the Earth's environment, space weather includes sudden changes (or disturbances) in the magnetosphere, ring current, radiation belts, geomagnetic field, auroras, ionosphere, and thermosphere. The disturbances in the geomagnetic field lasting from several hours to several days and produced by the intensification of magnetospheric current systems are called geomagnetic storms (Svalgaard 1977; Gonzalez et al. 1994; Lühr, et al. 2017). The current systems contribute differently to the storms in different latitudes; and the storms are therefore identified by the indices such as the low latitude Dst (disturbance storm-time) index (Sugiura 1964; Love & Gannon 2009), mid latitude Kp index, and high latitude AE index (e.g., Rostoker et al. 1995). Another index sometimes used is the rate of change of the horizontal component (dH/dt) of the geomagnetic field. The Dst storms arise mainly from the intensification of the ring current due to ICME-magnetosphere coupling and ionosphere-ring current coupling, the efficiency of which has been studied using solar wind and IMF data and models (e.g., Burton et al. 1975; Fok et al. 2001; Newell et al. 2007; Leimohn et al. 2010). The storms become more intense with the increase in the solar wind velocity V and strength of IMF Bz southward (e.g., Ebihara et al. 2005). Based on the minimum value of Dst (DstMin) reached during the storm main phase (MP), the storms are classified as moderate storms (-100 <DstMin≤-50 nT), intense storms (−250 <DstMin≤-100 nT), and super storms (DstMin ≤−250 nT) (e.g., Gonzalez et al. 1994).

Scientific analysis of solar storms and geomagnetic storms leads to fundamental understanding of the Earth's surrounding space weather (e.g., Gopalswamy et al. 2005; Kamide & Balan 2016). Application oriented analysis of the storms enables the assessment and mitigation of space weather hazards on satellite systems, satellite communication and navigation, electric power grids, tele-communication systems, etc. Of particular concern are the effects associated with extreme storms (e.g., Boteler 2001; Viljanen et al. 2010; Hapgood 2011; Pulkkinen 2007; Love et al. 2017). A space weather event similar to the Carrington event of 1859 September 01-02 (Carrington 1859) occurring at the present times could cause very serious impacts in today's high-tech society (e.g., Baker 2008; Schrijver et al. 2015; Eastwood et al. 2017). It is therefore important for both scientific and technological reasons to identify some parameters of the storms that can indicate their severity.

Conventionally, DstMin, maximum rate of change of Dst during MP $(dDst/dt)_{MPmax}$, and maximum values of Kp and AE (Kp_{max} and AE_{max}), all representing geomagnetic storm intensities, have been used for investigating the space weather in Earth's environment. However, while studying what determines the severity of the space weather (Balan et al., 2014) we realized that DstMin is an insufficient indicator of severe space weather (SvSW), as reported also by Cid et al. (2014). We define severe space weather

(SvSW) as causing the reported electric power outages and/or tele-communication failures and normal space weather (NSW) as not causing such severe effects in a 50-year period (1958-2007). Our studies also showed that the mean value of Dst during MP ($\langle Dst_{MP} \rangle$) can indicate the severity of space weather (Balan et al. 2016). $\langle Dst_{MP} \rangle$ can also be used as a better reference than DstMin in developing a scheme for forecasting SvSW using ICME velocity and magnetic field (Balan et al. 2017a). The derived parameter ($\langle Dst_{MP} \rangle$) will hereafter be called *IpsDst* (Section 2).

In the brief report (Balan et al. 2016), we introduced *IpsDst* indicating the *impulsive* (*Ips*) strength of Dst storms to distinguish between SvSW and NSW using only the super storms (DstMin ≤-250 nT) in Kyoto Dst data. No other data were used. The present paper investigates the capability of the important storm parameters in Dst, Kp, and AE indices to distinguish between the SvSW and NSW events reported occurring in a 50-year period (1958-2007). In addition to the conventional parameters mentioned above, the paper uses the IpsDst for the Dst storms automatically identified in the widely used Kyoto Dst and new (and improved) USGS Dst data in 1958-2007. The paper also uses the mean values of Kp and AE during MP ($<Kp_{MP}>$ and $<AE_{MP}>$) in the same 50-year period. The SvSW events include the event on 1972 August 04, which was missed in Balan et al. (2016) because it occurred during a non-super storm (DstMin -125 nT). It has puzzled the scientific community because all other SvSW events (including the Carrington event of 1859 September 01-02) occurred during super storms. The paper also explains the physical significance of IpsDst and discusses the physical mechanism leading to large IpsDst and SvSW using the solar wind and IMF data from the ACE (Advanced Composition Explorer) satellite available since 1998.

Section 2 describes the data and analysis. The results are presented and discussed in Sections 3 and 4. The SvSW events reported occurring in the 50-year period (1958-2007) and the Carrington SvSW event only are investigated. The SvSW events reported occurring prior to the Dst era (Davidson 1940; Cliver & Dietrich 2013; Ribeiro et al. 2016; Love & Coïsson 2016; Love 2018) are discussed in Section 4, though not investigated for the lack of Dst data. Minor technological problems such as capacitor stripping in power transformers (e.g., Kappenman 2003) will be included later by using high resolution IpsDst.

2. Data and Analysis

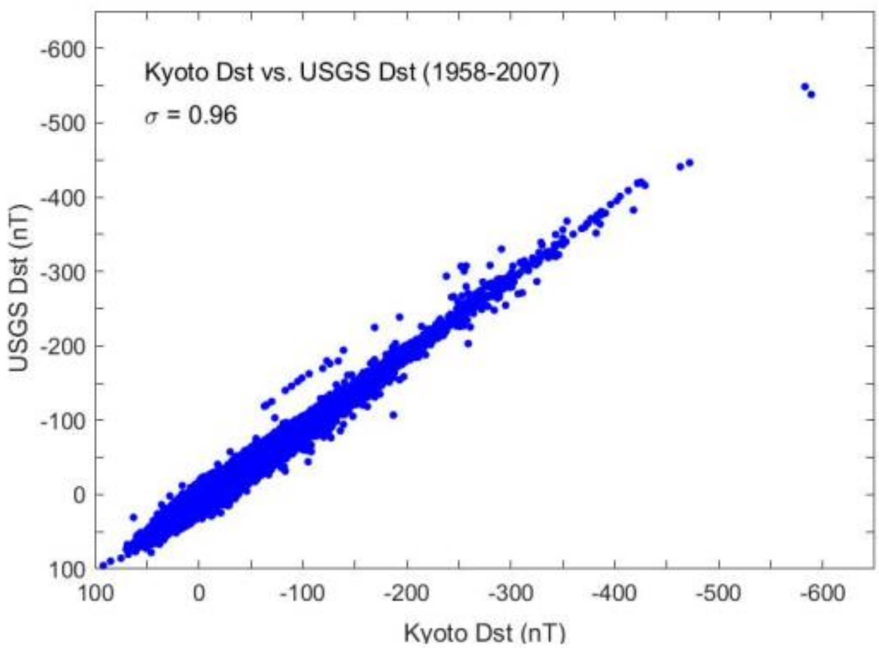

Figure 1. Scatter plot of hourly Kyoto Dst against USGS Dst in 1958-2007.

The hourly Kyoto Dst and USGS Dst data covering a 50-year time period (1958-2007) are available at http://wdc.kugi.kyoto-u.ac.jp/dstdir/ and http://geomag.usgs.gov/data, respectively. The primary difference between the Kyoto Dst (Sugiura 1964; Sugiura & Kamei 1991) and USGS Dst (Love & Gannon 2009) is in the removal of secular and solar quiet (Sq) variations. Kyoto Dst partially removes these variations while USGS Dst more fully removes them, which results in an offset between the two indices. Love & Gannon (2009) presented a panoramic view of the two indices for the whole 50-year period and detailed comparisons for selected 40-day time segments. They reported significant offset (Kyoto minus USGS) of up to -70 nT between the indices. Figure 1 shows a scatter plot of the indices in the 50-year period. The indices have a correlation of 0.96 and the offset is mainly negative. The average offset is -8.50 nT in all data together and -5.0 nT in quiet-time (Dst >-25 nT) data alone (Balan et al. 2017b). For the Carrington storm, the H-component data measured at Bombay (Tsurutani et al. 2003) and calculated by Cliver & Dietrich (2013) are used. The Kp and AE data are available at http://wdc.kugi.kyoto-u.ac.jp/kp/index.html and http://wdc.kugi.kyoto-u.ac.jp/aedir/, respectively.

The Dst storms were automatically identified by a computer program that uses four selection criteria. The criteria are (1) DstMin ≤ -50 nT and T_{MP} > 2 hours, (2) absolute value of MP range, that is, $|Dst_{MPO}$ -DstMin$|$ ≥ 50 nT, (3) separation between DstMin and next MPO ≥ 10 hours, and (4) rate of change of Dst during MP or $(dDst/dt)_{MP}$ <-5 nT/hr. MPO here stands for MP onset. The selection criteria minimize non-storm like fluctuations (Balan et al. 2017b). The computer program identified 761 storms in Kyoto Dst, which include 34 super storms, 296 intense storms, and 431 moderate storms. The

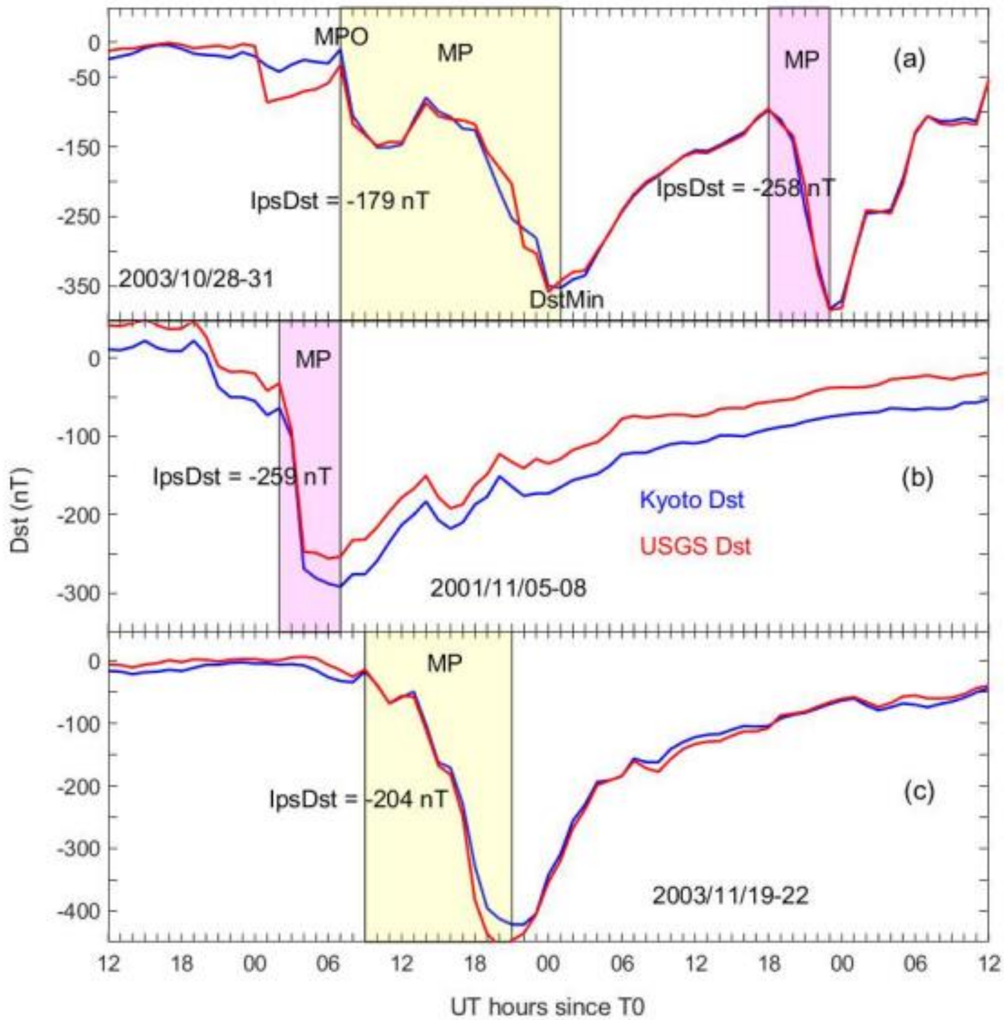

Figure 2. Comparison of four super storms (DstMin ≤-250 nT) in Kyoto Dst (blue) and USGS Dst (red) having large IpsDst (purple shade) and comparatively weak IpsDst (yellow shade). MPOs are identified by a computer program satisfying storm selection criteria and IMF Bz turning southward. The time T0 of X-axis corresponds to 12 UT on 2003 October 28 (panel a), 2001 November 05 (panel b), and 2003 November 19 (panel c), respectively.

585 storms identified in USGS Dst include 33 super storms, 210 intense storms, and 342 moderate storms. Figure 2 compares four super storms in the two indices. Intense and moderate storms were compared before (Balan et al. 2017b). Although the storms in the two indices exhibit similar variations, they have differences in DstMin and in its time of occurrence, which can cause differences in IpsDst.

2.1. Parameter IpsDst

The parameter *IpsDst* is defined as IpsDst = $(-1/T_{MP})\int_{TMP}|Dst_{MP}|dt$ (Balan et al. 2014). $\int_{TMP}|Dst_{MP}|dt$ is the integral (or sum) of the modulus of Dst from MPO to DstMin. MPO is the MP onset time when Dst starts decreasing satisfying the storm selection criteria (and IMF Bz turning southward) which is also the peak of the storm sudden commencement (SSC). T_{MP} is the time interval (or duration) from MPO to DstMin. The rate of change of Dst during the MP and its maximum value $(dDst/dt)_{MPmax}$ are obtained. By definition, the IpsDst includes most important characteristics of Dst storms (SSC, MPO, $(dDst/dt)_{MPmax}$, DstMin, and T_{MP}) and gives the mean value of Dst during the MP when most energy input occurs (Figure 2). IpsDst is proportional to the total amount of energy input during MP (e.g., Burton et al. 1975) divided by the duration of energy input. The higher the energy input and shorter the duration, the larger the IpsDst value and more impulsive its action, and so the name IpsDst. The maximum values of the Kp and AE storms (Kp_{max} and AE_{max}) are noted. Their MP durations corresponding to the MP of Dst storms are identified as shown by an example in Figure 3. The mean values of Kp and AE during the storm MP are calculated as

$$\langle Kp_{MP}\rangle = \Sigma Kp_{MP}/T_{MP} \quad \text{and} \quad \langle AE_{MP}\rangle = \Sigma AE_{MP}/T_{MP.}$$

$\langle Kp_{MP}\rangle$ and $\langle AE_{MP}\rangle$ might represent the impulsive strength of the Kp and AE storms because they give the mean values of Kp and AE during the storm MP when most energy input occurs.

The accuracy of IpsDst depends on the accuracy of the Dst data and T_{MP}. According to Sugiura (1964), who developed the Dst index, it is not easy to compute the uncertainty of Dst (T. Iyemori 2019, private communication). The uncertainty includes the

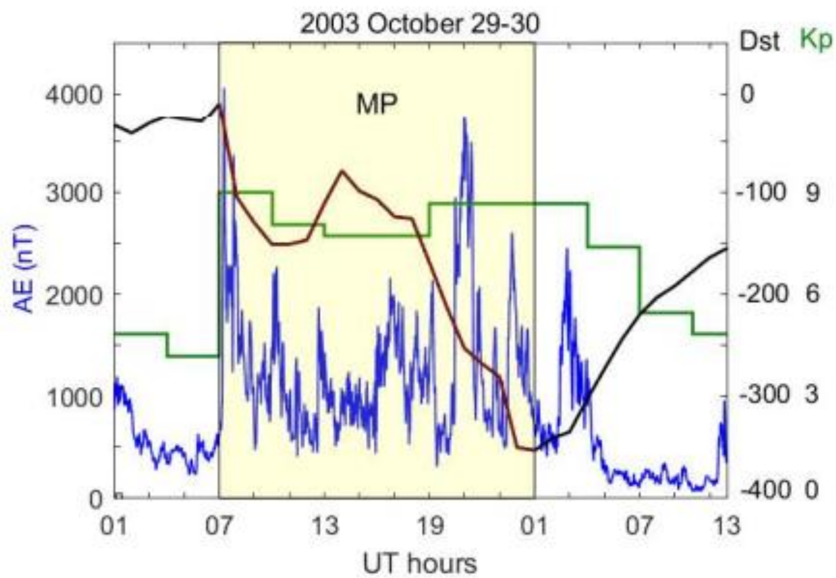

Figure 3. An example identifying the storm main phase MP in Dst, Kp, and AE storms.

measurement errors at the four Dst observatories, errors associated with the selection of 5 quiet days for each month, and errors due to the variation of quiet-time ring current when Dst is zero. These errors are mostly removed in the final version of Dst especially in USGS Dst (Love & Gannon 2009). The uncertainty also seems to depend on the time when a storm actually hits the Dst stations and the time when Dst shows the storm. However, this difference in time may not cause significant difference in Dst because the ring current starts developing not at a specific point in time but during a certain range in time (M. Nose 2019, private communication). The accuracy of T_{MP} depends on the accurate identification of the times of MPO and DstMin. The computer program identifies these times following the selection criteria. The MPO times of the storms since 1998, when ACE data are available, are also found agreeing with the times of IMF Bz turning southward. The time resolution (1 hour) of the Dst data, however, can cause significant uncertainty in IpsDst. It causes ±30 minutes uncertainty in the identification of MPO and DstMin or an uncertainty ΔT_{MP} of ±1 hour in $T_{MP.}$ The corresponding uncertainty in IpsDst is ΔIpsDst = ±IpsDstx($\Delta T_{MP}/T_{MP}$). Table 1 lists the computed IpsDst and its uncertainty of all 35 super storms and the intense storm on 1972 August 04. It assumes that the uncertainty in Dst is negligible compared to that in $T_{MP.}$ The uncertainty in general decreases with increasing (negative) IpsDst.

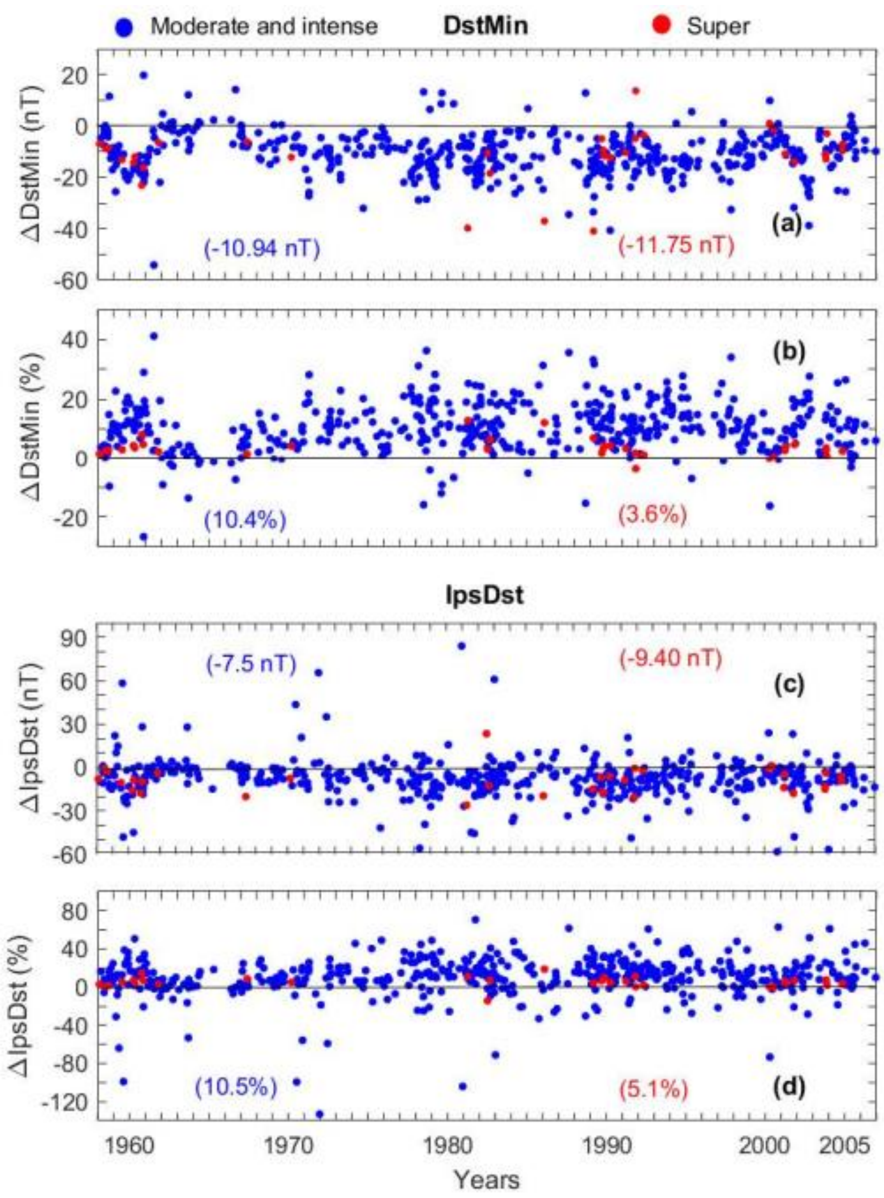

Figure 4. Scatter plot of the absolute and percentage differences (Kyoto minus USGS) in DstMin (a and b) and IpsDst (c and d) of the storms in the two Dst indices as function of time, with red color for super storms and blue color for intense and moderate storms together. The average differences are noted inside brackets.

Table 1: Number, dates, and parameter values in the order of IpsDst in Figure 6

No. & Date	-IpsDst (nT) (nT)	T_{MP} (hrs)	-DstMin (nT)	$(dDst/dt)_{MPmax}$ (nT/hr)	F10.7	SvSW/NSW
1. 1859-09-01	700±100	2	1710	1390	nan	SvSW
2. 1989-03-13	357±22	16	589	111	253	SvSW
3. 1958-02-11	275±34	8	426	103	224	SvSW
4. 2001-11-06	259±52	5	292	168	233	SvSW
5. 2003-10-30	258±52	5	383	98	268	SvSW
6. 2001-03-31	238±48	5	387	148	245	NSW
7. 1981-04-13	235±34	7	311	75	255	NSW
8. 1967-05-26	230±19	12	387	106	219	NSW
9. 2004-11-10	229±25	9	263	43	103	NSW
10. 1989-10-21	220±20	11	268	61	206	NSW
11. 1960-04-01	217±24	9	327	56	201	NSW
12. 2004-11-08	209±19	11	374	96	122	NSW
13. 2003-11-20	204±17	12	422	100	171	NSW
14. 1959-07-15	204±19	11	429	92	253	NSW
15. 1958-09-04	201±22	9	302	55	261	NSW
16. 1991-10-29	188±24	8	254	29	269	NSW
17. 1991-11-09	187±16	12	354	61	194	NSW
18. 1960-04-30	184±31	6	325	151	164	NSW
19. 2000-04-06	183±23	8	288	74	178	NSW
20. 2003-10-29	179±10	18	353	95	275	NSW
21. 1989-11-17	179±14	13	266	52	215	NSW
22. 1982-09-06	174±15	12	289	44	172	NSW
23. 2000-07-15	172±19	9	301	137	220	NSW
24. 1958-07-08	170±13	13	330	92	240	NSW
25. 1982-07-14	163±18	9	325	110	269	NSW
26. 1991-03-25	157±16	10	298	63	235	NSW
27. 1970-03-08	156±20	8	284	90	173	NSW
28. 1961-10-28	154±17	9	272	62	86	NSW
29. 2001-04-11	145±18	8	271	58	160	NSW
30. 1960-11-13	142±8	17	339	81	178	NSW
31. 1990-04-10	133±7	20	281	45	149	NSW
32. 1960-10-07	120±4	28	287	45	145	NSW
33. 1972-08-04	112±22	5	125	35	125	SvSW
34. 1992-05-10	111±6	18	288	62	127	NSW
35. 1989-09-19	106±8	14	255	40	197	NSW
36. 1986-02-08	105±2	47	307	71	94	NSW

Table 1. Table lists the storm numbers and dates of IpsDst in Figure 6a and corresponding other parameters including SvSW/NSW. IpsDst (column 2) includes its uncertainty (limited to ±100 nT for the Carrington event). The values of the other parameters in Figure 6 do not correspond to the same number and date because of their increasing or decreasing ordering.

The offset between the two Dst indices causes differences in their storm parameters. Figure 4 shows the absolute and percentage differences (Kyoto minus USGS) in DstMin and IpsDst of the storms as function of time, with red color for super storms and blue color for intense and moderate storms together. Though the absolute difference is mainly negative up to -54 nT in DstMin (Figure 4a) and -58 nT in IpsDst (Figure 4c), it is also positive up to 20 nT in DstMin and 84 nT in IpsDst for a small number of storms. The percentage difference is positive up to 40% in DstMin (Figure 4b) and 65% in IpsDst (Figure 4d) though it is negative up to -35% in DstMin and -130% in IpsDst for a small number of storms. The average differences noted in the figure are smaller in IpsDst than DstMin by about 2 nT on the whole, though their percentage differences are nearly equal. T_{MP} (not shown) is found equal for about half of the storms and differs for others resulting in an average difference of -0.28 hours overall. T_{MP} differs generally due to the DstMin in one index occurring slightly later or earlier compared to the other index (Figure 2). As discussed, there are significant offsets between the two Dst indices and differences in their storm parameters. It therefore becomes interesting to investigate how well the various important storm parameters in the two Dst indices and Kp and AE indices work in distinguishing between the SvSW and NSW events.

The ACE satellite at the L1 point has provided IMF and solar wind data continuously since 1998. The velocity and density data in the SWI (Solar Wind Ion) mode of the SWEPAM (Solar Wind Electron Proton Alpha Monitor) instrument at 64-second resolution (e.g., McComas et al. 1998; Skoug et al. 2004) are available at Caltech (http://www.srl.caltech.edu/ACE/ASC/). During high energy particle events, when the

SWI mode may not cover the full solar wind flux distribution, the 64-second data collected in the SSTI (Search/Supra Thermal Ion) mode once every ~32 minutes will be used. The data (time) is corrected for the ACE-Earth distance. The velocity and IMF data for the Carrington, Quebec, 1958 February, and 1972 August events are adopted from the calculations by Cliver & Svalgaard (2004), Nagatsuma et al. (2015), Cliver et al. (1990), and Vaisberg & Zastenker (1976), respectively.

For discussing the mechanism connecting the Dst storms and solar storms (Section 4.3), we define the beginning of an ICME event as the time when the solar wind velocity (V) suddenly increases to high values (Balan et al. 2014). The ICME event front (or shock) velocity ΔV is the difference between the peak ICME velocity and the upstream slow solar wind velocity (V). The velocity, especially during severe events measured with 32-minute resolution, is found to take about two hours to reach its peak. ΔV in general is therefore taken as the difference between the mean velocity for 2 hours after and 2 hours before the start of the velocity increase. Bz at ΔV ($Bz_{\Delta V}$) is the mean of Bz for the two hours from the start of the velocity increase.

3. Identification of SvSW

3.1. Definition and events

As mentioned in Section 1, the space weather events reported to have caused electric power outages and/or telegraph system failures in the 50-year period (1958-2007) are defined as *severe space weather (SvSW)*. Five such SvSW events are reported occurring in 1958-2007. The event of 1958 February 11 damaged telegraph systems in Sweden (e.g., Wik et al. 2009) and caused electric power supply problems in the US

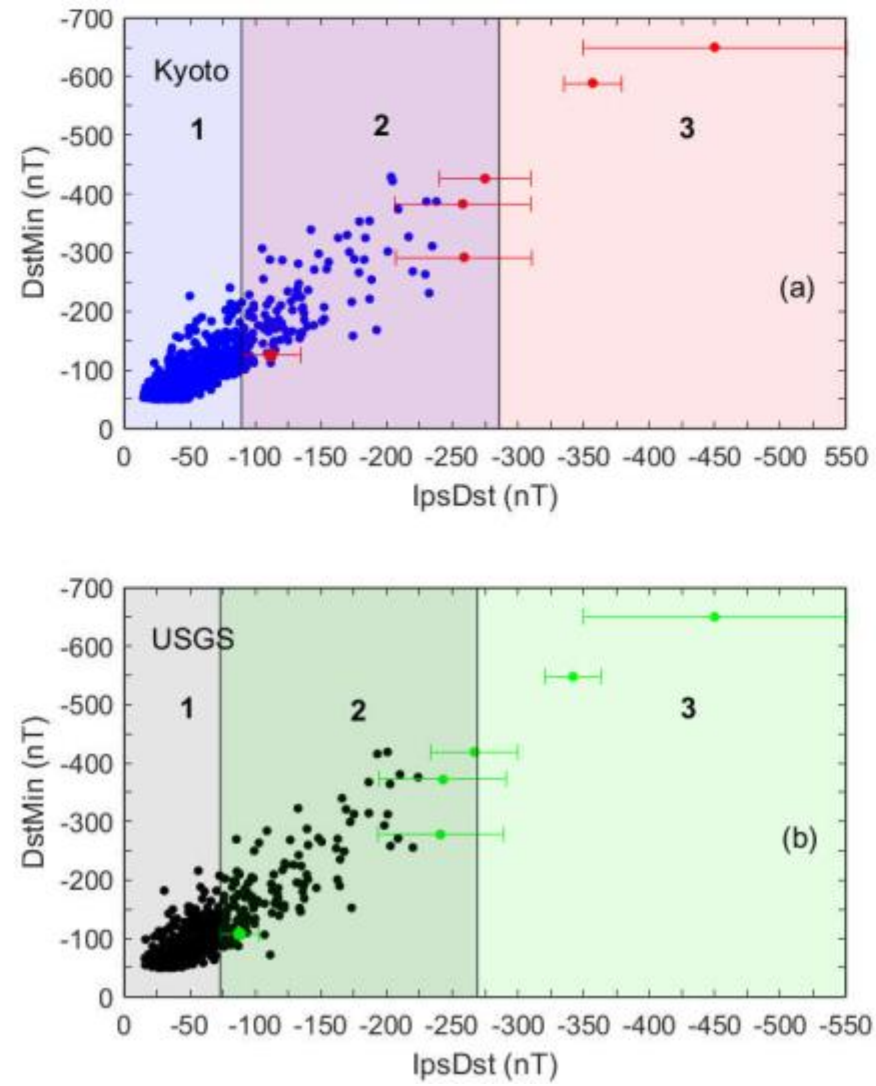

Figure 5. Scatter plot of IpsDst against DstMin of the Carrington storm and all common storms during 1958-2007 in (a) Kyoto Dst and (b) USGS Dst. Red and green dots correspond to SvSW events. Regions 1-2 and 2-3 represent the IpsDst ranges of NSW and SvSW events including the uncertainty in IpsDst due to the uncertainty in T_{MP} of the respective highest and lowest IpsDst values. The horizontal bars show the uncertainty in IpsDst of the SvSW events only for simplicity and limited to ±100 nT for the Carrington event.

(Slothower & Albertson 1967). The event of 1972 August 04 caused tele-communication failure and electric power supply problems in the US (Anderson et al.1974; Albertson & Thorson 1974). The Quebec event of 1989 March 13 (e.g., Medford et al. 1989) and the New Zealand event of 2001 November 06 (Marshall et al. 2012) caused electric power outages. The Halloween event of 2003 October 30 caused an electric power outage in Sweden (e.g., Pulkkinen et al. 2005). The Carrington event of 1859 September 01-02 that caused telegraph system failures (Loomis 1861) is also included. All other space weather events occurred in the 50-year period are considered normal space weather (NSW) events because they are not reported to have caused such severe effects.

3.2. Identification

Using DstMin and IpsDst, we attempt to determine their abilities to differentiate between SvSW and NSW events for each of the two Dst indices. Figure 5 shows scatter plots of IpsDst against DstMin considering all common storms in 1958-2007. For the Carrington storm (right-hand top event), the equivalent DstMin and IpsDst are limited to -650 nT and -450 nT, respectively. Red and green colors represent SvSW in Kyoto Dst and USGS Dst, respectively. The regions marked 1-2 and 2-3 represent the IpsDst ranges of NSW and SvSW events including the uncertainty in IpsDst due to the uncertainty in T_{MP} of the respective highest and lowest IpsDst values. IpsDst, seems able to mostly differentiate between the populations of SvSW and NSW in both Dst indices. Using DstMin only allows for the separation of 2 out of the 6 events. Due to the lone SvSW event (1972 August 04) that is not separated by IpsDst, there appears a very wide range of IpsDst that can cause SvSW and the distribution overlaps with that of NSW. We will discuss the 1972 August 04 SvSW event in Section 4.1.

Next, we include other important storm parameters. Though we analysed all storms, the parameters are shown only for all super storms, the intense storm of 1972 August 04, and the Carrington storm. Figure 6 displays the IpsDst, T_{MP}, DstMin, and $(dDst/dt)_{MPmax}$

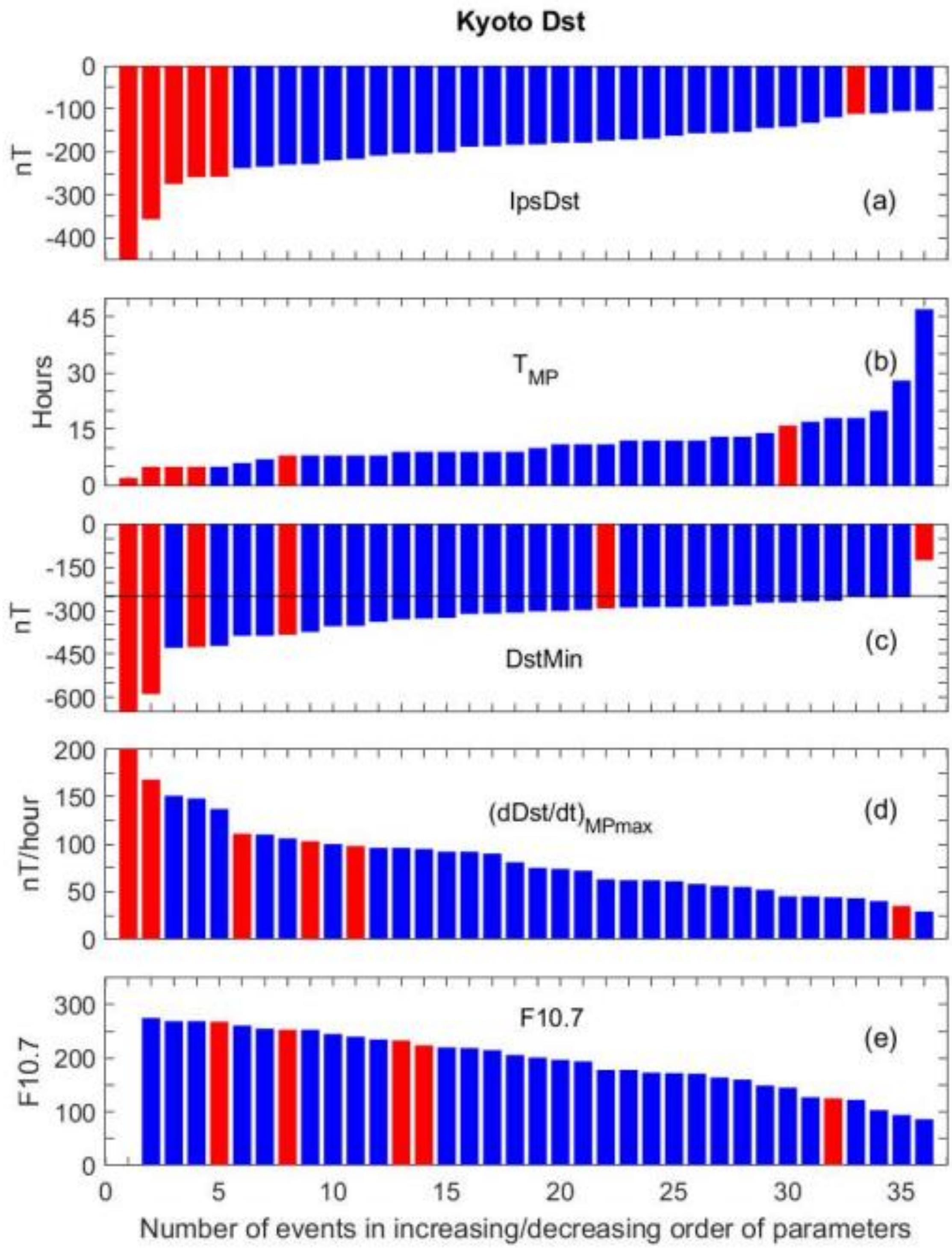

Figure 6. IpsDst, T_{MP}, DstMin, $(dDst/dt)_{MPmax}$, and F10.7 on the days of DstMin of the super storms (DstMin ≤-250 nT) in Kyoto Dst arranged in their increasing or decreasing orders. The Carrington storm of 1859 and intense storm on 1972 August 04 are included. Red color corresponds to SvSW and blue color to NSW (see text).

in Kyoto Dst; the solar activity index F10.7 on the days of DstMin is also shown. For the Carrington event (number 1), the equivalent DstMin, IpsDst, and $(dDst/dt)_{MPmax}$ are limited to -650 nT, -450 nT, and 200 nT/hr, respectively, for better display with other parameters in the figure. All parameters are arranged in their respective increasing or decreasing orders. Red and blue colors represent SvSW and NSW events, respectively. Table 1 lists the IpsDst together with its uncertainty and other parameters for each of the storms shown in Figure 6. IpsDst best sorts out SvSW from NSW, despite the outlier of event number 33 (1972 August 04) having significantly weak IpsDst (-112 nT), which will be discussed in Section 4.1.

Figure 7 is similar to Figure 6 but for USGS Dst with green and black colors representing SvSW and NSW events, respectively. The offset between the two Dst indices results in the absence of one super storm in USGS Dst. The differences in the respective storm parameter values between the two indices result in some differences in the order number of the parameters in Figure 7 compared to Figure 6. For these reasons, F10.7 is also shown in Figure 7. The behavior of all parameters in USGS Dst is similar to that in Kyoto Dst.

3.3. Kp and AE indices

Since SvSW effects usually occur at high latitudes, one might expect the high and mid latitude indices (AE and Kp) could also be used to distinguish between SvSW and NSW events. However, these indices are inadequate as illustrated in Figure 8, which shows $\langle Kp_{MP} \rangle$, Kp_{max}, $\langle AE_{MP} \rangle$, and AE_{max} corresponding to the Dst storms in Figure 6a. The parameters are arranged in their respective decreasing orders. Red and blue colors

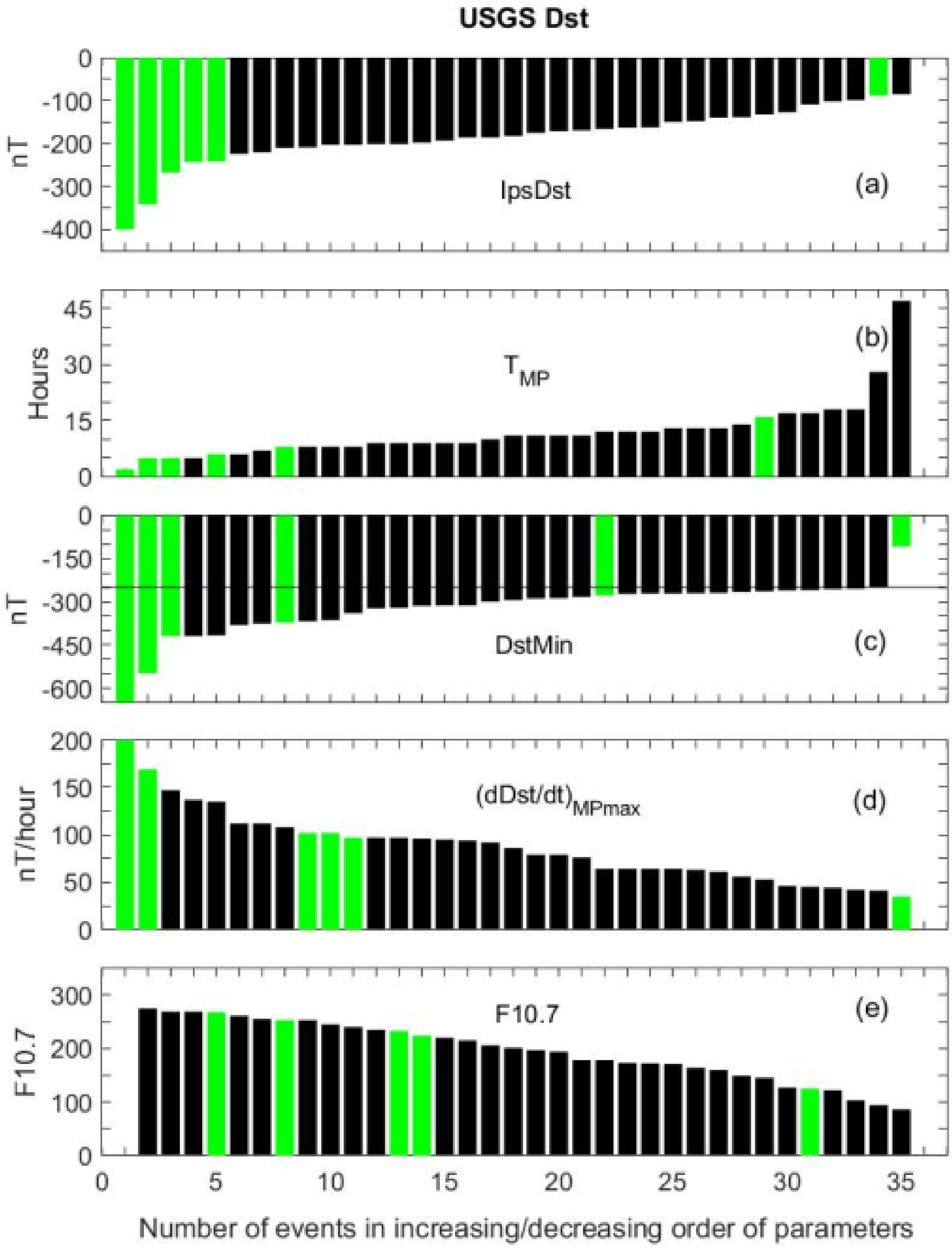

Figure 7. IpsDst, T_{MP}, DstMin, $(dDst/dt)_{MPmax}$, and F10.7 on the days of DstMin of the super storms (DstMin ≤-250 nT) in USGS Dst arranged in increasing or decreasing orders of the parameters. The Carrington storm of 1859 and intense storm on 1972 August 04 are included. Green color corresponds to SvSW and black color to NSW (see text).

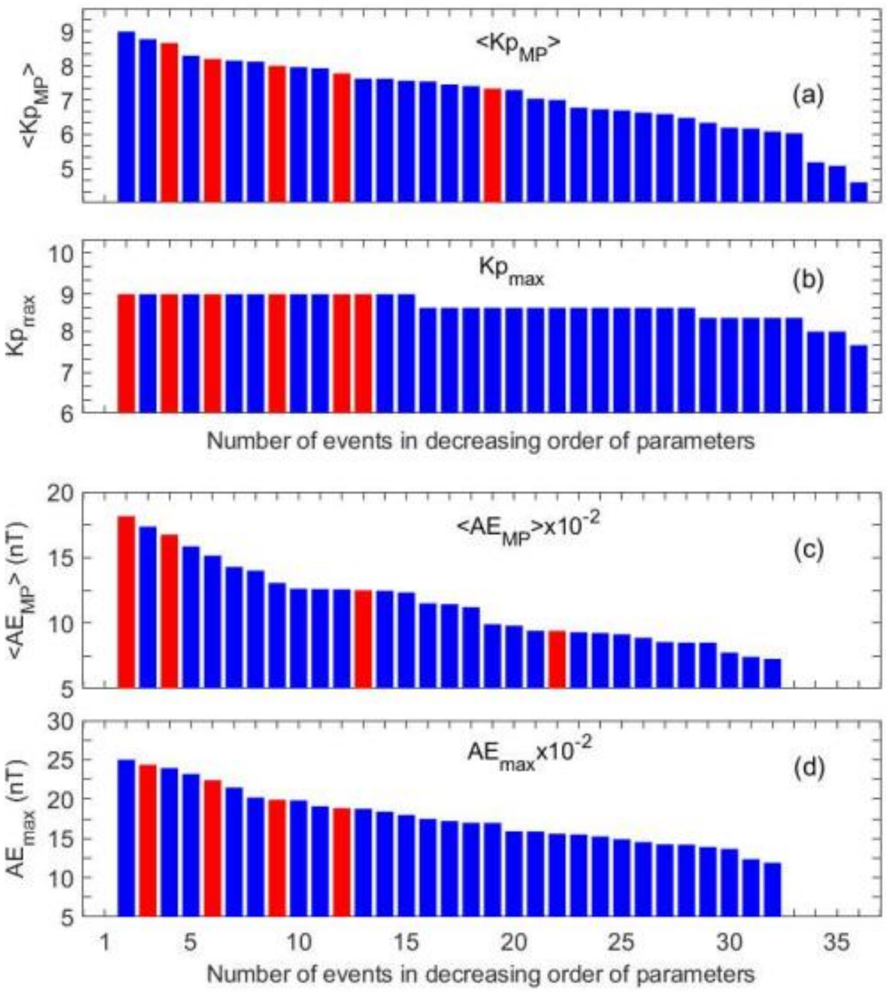

Figure 8. $\langle Kp_{MP} \rangle$, Kp_{max}, $\langle AE_{MP} \rangle x10^{-2}$, and $AE_{max}x10^{-2}$ arranged in their decreasing orders. The parameters correspond to the Dst storms shown in Figure 6a. The Carrington event has no Kp data and five events including the Carrington and 1972 August 04 events have no AE data. Red and blue colors correspond to SvSW and NSW, respectively.

correspond to SvSW and NSW, respectively. In Figure 8a, the SvSW events from left to right correspond to the storms in 2001 November, 2003 October, 1958 February, 1989 March, and 1972 August, respectively. The Carrington event has no Kp data and five events including the Carrington and 1972 August 04 events have no AE data. In all parameters (Figure 8), the SvSW events are mixed with NSW events. AE and Kp seem inadequate to distinguish between SvSW and NSW mainly because they do not distinguish their phases when a majority of energy input occurs. Kp is also a 3-hour index, and AE can sometimes reach maximum before the main energy input starts from the MPO of Dst storms.

4. Discussion

As mentioned in Section 1, Dst storms have been studied and modeled for many years using Dst index, solar wind, and IMF data. The models have improved our understanding of the mechanisms connecting Dst storms and solar storms. For example, using V, N (density), and Bz, Burton et al. (1975) modeled the seven Dst storms in 1967–1968. Klimas et al. (1997) presented a method for transforming a linear prediction model into linear and non-linear dynamical analogues of the coupling between the input and output data. Using VBz for input and Dst for output, they showed that the non-linear analogue couples to the solar wind through the expression (VBz/Dst)×VBz rather than through the usual linear dependence on VBz. The multi-input (VBz and dynamic pressure P) and single-output (Dst) discrete time model developed by Zhu et al. (2007) explains the Dst dynamics more accurately than previous models. Using USGS Dst and a lognormal stochastic process, Love et al. (2015) reported that the most extreme Dst storms (DstMin ≤ -850 nT) can occur ~1.13 times per century, with 95% confidence level. The ICME-magnetosphere coupling function developed by Newell et al. (2007) is a good measure of the coupling efficiency, though is still not able to distinguish between SvSW and NSW (Balan et al. 2017a).

By definition, the parameter IpsDst = $(-1/T_{MP})\int_{TMP}|Dst_{MP}|dt$ gives the mean value of Dst duirng storm MP (Figure 2), and therefore indicates the impulsive strength of Dst storms

Table 2 : Truth table

Total = 762	**Identified**	
	True	**False**
Actual SvSW	a = 5	b = 0
Actual NSW	c = 756	d = 1

Table 2: The truth table lists the number of (a) true SvSW, (b) false SvSW, (c) true NSW, and (d) false NSW events identified by IpsDst for a threshold of -250 nT in Kyoto Dst.

(IpsDst). The important result from Section 3 is that, irrespective of the significant offset and differences between the two Dst indices, the impulsive parameter IpsDst in both indices seems more likely to distinguish between SvSW and NSW events than other common Dst-based parameters. Using a truth table, we calculate the success of the identification. Table 2 lists the number of (a) true SvSW, (b) false SvSW, (c) true NSW, and (d) false NSW identified by IpsDst for a threshold of -250 nT in Kyoto Dst. Following Kohavi & Provost (1998), we calculate an accuracy [(a+c)/(a+b+c+d)] of 99.9% for the identification of SvSW and NSW events together and a true SvSW identification rate [a/(a+b)] of 100% with only one false NSW. The false NSW corresponds to the event on 1972 August 04 having small IpsDst, which is actually a SvSW event (Figure 5). We discuss this event in greater detail below.

4.1. SvSW Event on 1972 August 04

As reported by Anderson et al. (1974) and Albertson & Thorson (1974), a communication cable system outage and electric power supply problems occurred in the US during the rapid changes in the magnetic field during the large geomagnetic storm on 1972 August 04. Though no solar wind and IMF data were available, measurement of the time delay between the solar flare onset and shock arrival at 1 AU gives the fastest ever recorded speed of ~2850 km s^{-1} for the ICME shock (Vaisberg & Zastenker 1976) which might have compressed the magnetopause to ~5Re (Anderson et al. 1974; Lanzerotti 1992). Study of the Pioneer 10 data at ~2 AU showed that the average IMF Bz was around zero with considerable north-south fluctuations, and the geomagnetic storm was probably caused by a southward Bz fluctuation following the fast ICME shock (Tsurutani et al. 1992). The calculations by Tsurutani et al. (1992), assuming a solar wind speed of 2000 km s^{-1} and magnetopause compression to 5Re, show large storm-time ring current peak intensity corresponding to -295 nT. Kp reached its highest values of 9; AE data are not available. Model calculations by Boteler & Beek (1999) showed that the outages were due to a rapid intensification of the electrojet current as is typical for other SvSW events. The high impulsive action of the fastest ICME shock followed by the short-duration Bz southward seems to account for this SvSW event. If Bz had been southward for a longer period covering the ICME shock or ICME front, this event could have caused devastating effects.

The Dst storm (Figure 9d) has MPO at 23 UT (Dst -45 nT in Kyoto Dst) and DstMin (-125 nT) at 04 UT giving a T_{MP} of 5 hours and IpsDst of -112 nT, which is low compared to the IpsDst of other SvSW events. The hourly values of the corresponding H components (Figure 9c) used for calculating Dst also have low H ranges ($\triangle$H = 52-92 nT) though their durations (1-2 hours) are short compared to T_{MP} (5 hours). To better understand the IpsDst value, the H component magnetograms at the Dst stations Kakioka and San Juan available at http://wdc.kugi.kyoto-u.ac.jp/film/index.html are manually scaled four times at 5-minute intervals. The scaled values are digitized using

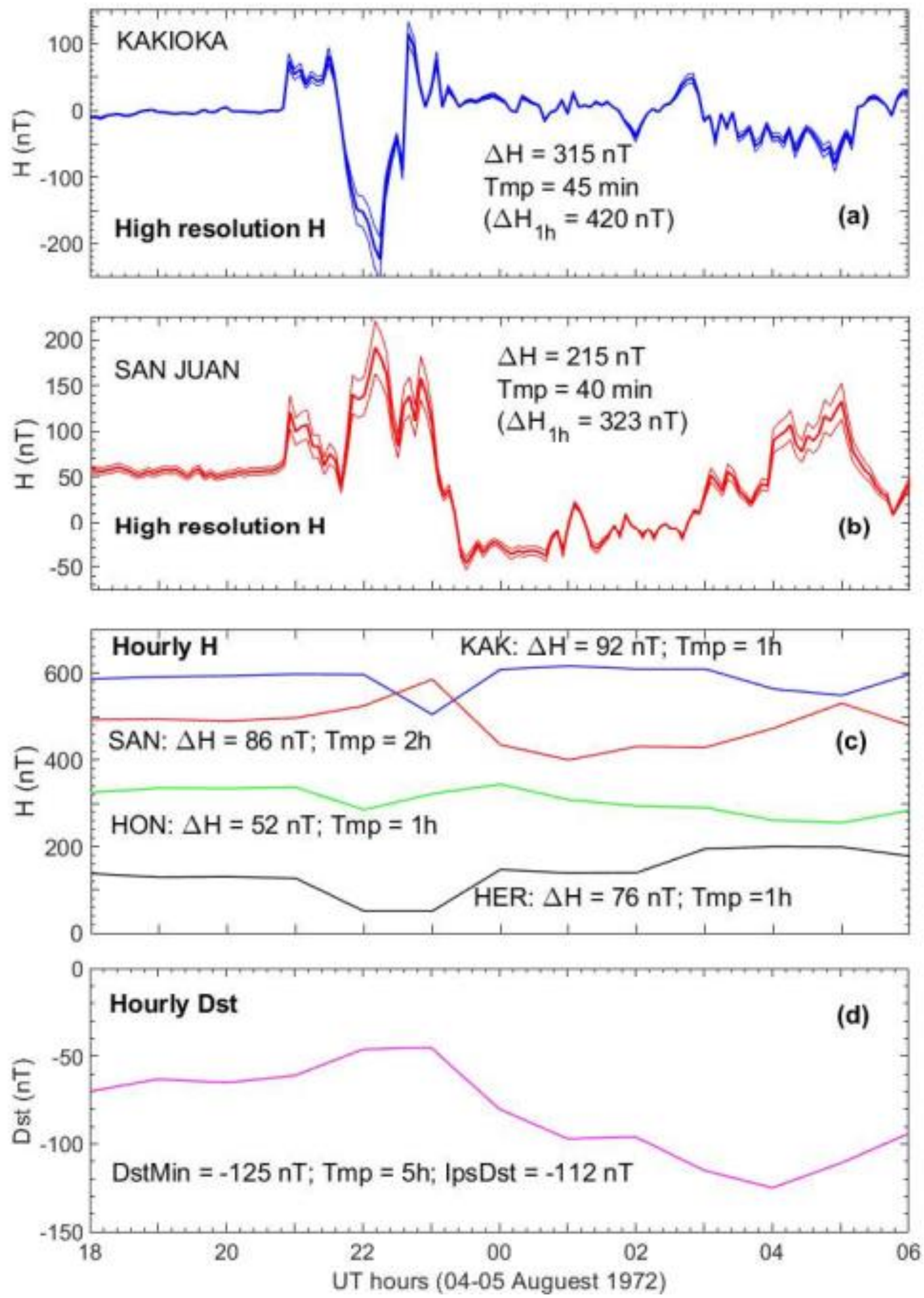

Figure 9. Scaled values (5-minute resolution) of the H component magnetograms on 1972 August 04-05 at the Dst stations (a) Kakioka and (b) San Juan with standard deviations; zero corresponds to baseline levels of 30094 nT and 27440 nT, respectively. The corresponding (c) hourly H values at all four Dst stations used for computing the (d) Dst index are shown. Important parameter values are listed.

the baseline values of 30094 nT and 27440 nT, respectively, and scale conversion factors provided by the observatories (M. Nose, 2018, private communication). The 4 H values at each time step are used to obtain their mean and standard deviation (up to ~15%). The time variations of H (Figures 9a and 9b) show large $\triangle$H over very short durations (315 nT in 45 minutes at Kakioka and 215 nT in 40 minutes at San Juan) translating to $\triangle H_K$ of 420 nT and $\triangle H_S$ of 325 nT in 1 hour. The $\triangle$H values are used to calculate Dst (Sugiura & Kamei, 1991) as Dst = $(1/2)(\triangle H_K/\cos(26.0)+\triangle H_S/\cos(29.9))$ with 26.0 and 29.9 being the dip latitudes at Kakioka and San Juan. It gives 1-hour Dst (and IpsDst) of ~-421 nT. This is an approximate value because we could not use the magnetograms at Honolulu and Hermanus, which have poor quality, and could not apply the Sq correction, which requires H values for previous five years.

To check the effect of high resolution data further, we use the SymH index available since 1981 at http://wdc.kugi.kyoto-u.ac.jp/aeasy to calculate IpsSymH. It is similar to IpsDst but calculated for the SymH index of 1-minute resolution derived using the H component data from 12 low latitude stations (Iyemori et al. 1991). The distribution of IpsSymH (not shown) is similar to that of IpsDst (Figure 5); and it appears that IpsSymH may be superior to IpsDst in its ability to distinguish between SvSW and SNW. Further studies using high resolution Dst (at least since 1958) are required to calculate the likelihood that a given IpsDst will actually cause SvSW or NSW, which is planned as described below.

4.2. SvSW Events Prior to Dst era

In addition to the SvSW events in 1958-2007 and the Carrington event investigated in Section 3, the SvSW events reported occurring prior to the Dst era also seem to agree with the criterion of large IpsDst. Love (2018) reported widespread problems that occurred in telegraph and telephone systems in the US on 1882 November 17. The simultaneous magnetograms recorded at the nearby station Los Angeles (40.88˚N magnetic) showed a 1-hour average $\triangle H$ of 470 nT, T_{MP} of 5 hours, and large dH/dt. Using Bombay magnetograms, they (Love 2018) estimated a DstMin of -386 nT. The aa index, which is a simple 3 hourly global geomagnetic activity index available since 1868 and derived from two approximately antipodal observatories in Australia and UK (Mayaud 1972), averaged to its highest value of 215 nT. These characteristics indicate a large IpsDst (<-250 nT). Ribeiro et al. (2016) described widespread problems occurring in the telegraph communication networks in two mid-latitude countries (Portugal and Spain) on 1903 October 31. The magnetic field recorded simultaneously in these countries showed a large storm (similar to the Quebec storm of 1989 March 13) with H ranges over 500 nT and large dH/dt indicating that the corresponding IpsDst could have been <-250 nT. As reviewed by Cliver & Dietrich (2013), the event on 1921 May 14-15 caused telephone cable burning in Sweden and a fire at the Central New England Railroad Station switchboard in the US. Based on simultaneous magnetograms, Kappenman (2006) estimated DstMin ~-850 nT for this storm, which indicates a large IpsDst. The magnetic storms on 1940 March 24 and 1941 September 19 which caused electric power supply and tele-communication problems in the US (Davidson 1940 and Love & Coïsson, 2016) and when Kp reached 9 are also estimated to have large IpsDst and DstMin (<-250 nT) (unpublished Dst data, J. J. Love 2018, private communication).

We plan to digitize the analogue magnetograms available since 1904 at the four Dst stations at high time resolution (e.g., 5-minutes), compute the Dst data, automatically identify the Dst storms, and obtain the IpsDst and other important storm parameters. The magnetograms available at Cape Town will be used for the period prior to 1940 when the same are not available for the closest Dst station Hermanus. We will study how well the high-resolution storm parameters work in identifying the reported SvSW events including minor technological problems since 1904. We expect that the high resolution IpsDst will enable us calculate the likelihood that a given IpsDst will actually cause SvSW or NSW. In short, the high resolution IpsDst could be a very useful parameter for investigating different aspects of space weather.

4.3. Physical Mechanism

The mechanism of large IpsDst (high energy input over a short duration) probably takes place through continuous and rapid magnetic reconnection (e.g., Borovsky et al. 2008). This important physical process seems to happen when there is a simultaneous occurrence of high solar wind velocity V (>~700 km s^{-1}) coupled with a high ICME front velocity ΔV (sudden increase by over 275 km s^{-1}) and sufficiently large IMF Bz southward during the velocity increase ΔV (Balan et al. 2014). The importance of the coincident velocity increase and IMF Bz southward is illustrated in Figure 10. It displays the IpsDst of the 13 super storms (in Kyoto Dst) since 1998, Carrington super storm, and 1972 August 04 storm (number 15) and corresponding ICME and IMF drivers in increasing order of IpsDst. The $\langle V_{MP} \rangle$ of the Carrington and 1972 August 04 SvSW events is limited to 1600 km s^{-1} and their △V is limited to 1200 km s^{-1}. The solar wind velocity and IMF Bz data for the Carrington, Quebec, 1958 February, and 1972 August events (numbers 1-3 and 15) are adopted from the theoretical calculations by Cliver &

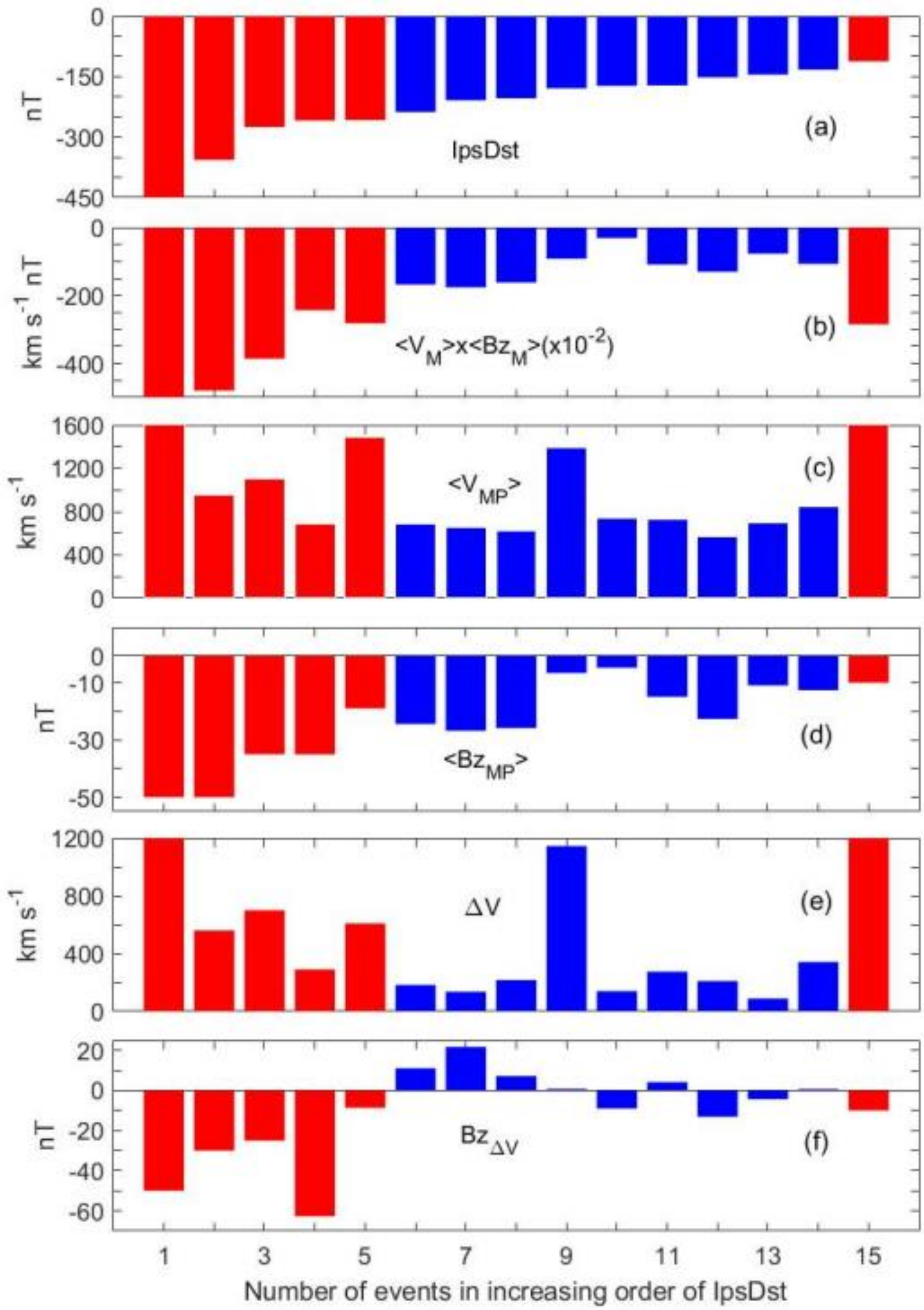

Figure 10. IpsDst of the super Dst storms (Kyoto Dst) since 1998, Carrington storm (number 1), and 1972 August storm (number 15) and corresponding $\langle V_{MP} \rangle x \langle Bz_{MP} \rangle$, $\langle V_{MP} \rangle$, $\langle Bz_{MP} \rangle$, $\triangle V$, and $Bz_{\triangle V}$ obtained from ACE data and adopted from theoretical values available in the literature (see text). All parameters are arranged in increasing order of IpsDst with red color for SvSW.

Svalgaard (2004), Nagatsuma et al. (2015), Cliver et al. (1990), and Vaisberg & Zastenker (1976), respectively. An IMF Bz of -10 nT is assumed for the 1972 August 04 event following Tsurutani et al. (1992).

The red histograms correspond to SvSW and blue histograms to NSW. As shown, IpsDst has (nearly) the same distribution as the product $\langle V_{MP}\rangle x\langle Bz_{MP}\rangle$ (Figures 10a and 10b) except for the event number 15 (1972 August 04) due to its high $<V_{MP}>$. The SvSW events 1-5 and 15 have both high $\langle V_{MP}\rangle$ (Figure 10c) and large $\langle Bz_{MP}\rangle$ southward (Figure 10d), as well as high ΔV (Figure 10e) and $Bz_{\Delta V}$ southward during the time of large ΔV (Figure 10f). Their combined action leads to large IpsDst. $\langle Bz_{MP}\rangle$ southward opens the dayside magnetopause and high ΔV (and high $\langle V_{MP}\rangle$) provides the force for the impulsive entry of a large number of high-energy charged particles into the magnetosphere and ring current. For NSW events (blue), the product $\langle V_{MP}\rangle x\langle Bz_{MP}\rangle$ is comparatively small. Their striking difference compared to SvSW events is small ΔV (except for the events 9 and 14) and Bz generally northward at the time of ΔV, so that either their impulsive action is weak or the strong action becomes ineffective. The coincidence of high $\langle V_{MP}\rangle$ with high ΔV and simultaneous large $\langle Bz_{MP}\rangle$ southward leading to a steep decrease of Dst and large IpsDst was modeled (Balan et al. 2017a) using the CRCM (comprehensive ring current model) of Fok et al. (2001). The model also showed that a high $\langle V_{MP}\rangle$ not associated with a large ΔV and large $\langle Bz_{MP}\rangle$ southward does not lead to large IpsDst. In Figure 10, the 1972 August 04 SvSW event is identified by $\langle V_{MP}\rangle x\langle Bz_{MP}\rangle$ but not by IpsDst because IMF Bz remained southward only for a short duration less than 1 hour as discussed in Section 4.1. It is also worth noting that while IpsDst is useful for identifying SvSW in ground data, the solar parameter VxBz showing a sharp negative spike exceeding a threshold is useful for forecasting SvSW with a maximum warning time of ~35 minutes using ACE satellite data (Balan et al. 2017a).

The coherence of the global parameters (high ΔV and large Bz southward) leading to another global parameter (large IpsDst) and a regional phenomenon (SvSW) reveals an impulsive solar wind-magnetosphere-ionosphere coupling, which seems essential for SvSW (Figure 10). The impulsive coupling results in an intense regional ionospheric current somewhere at high latitudes (e.g., Boteler & Beek, 1999), which generates strong magnetic fields reaching down to earth, which, in turn, induce strong currents and voltages in Earth systems (e.g., Viljanen et al. 2010). Such induced currents and voltages exceeding the tolerance limits of the systems cause system failures (e.g., Albertson et al. 1974; Lanzerotti 1983). Finally, it should be mentioned that the global parameter IpsDst can do only its job of identifying SvSW and it cannot indicate the time and location of the system damages that depend also on the regional ionospheric and ground conductivities and characteristics of the systems (power girds and tele-communication networks).

Summary

1. The parameter IpsDst = $(-1/T_{MP})\int_{TMP}|Dst_{MP}|dt$ gives the mean value of Dst during the storm MP. Its value decreases with increasing energy input ($\int_{TMP}|Dst_{MP}|dt$) and decreasing duration of energy input (T_{MP}), and therefore indicates the impulsive strength of Dst storms while DstMin and $(dDst/dt)_{MPmax}$ represent only their intensity at a single point in time.

2. IpsDst captures many important processes (ICME shock, magnetopause compression, SSC and energy input) related to the physical mechanism (high energy input over a short duration) causing the sudden intensification of high latitude ionospheric currents leading to severe space weather (SvSW) resulting in electric power outages and tele-communication system failures.

3. IpsDst is derived for the Dst storms automatically identified in Kyoto Dst and USGS Dst data for a period of 50 years (1958-2007). The IpsDst in both indices seems distinguishing 4 of the 5 SvSW events (and the Carrington event) from over 750 NSW events occurred in 1958-2007 though the indices have significant offset of up to -70 nT in Dst and differences of up to -54 nT in DstMin and -58 nT in IpsDst. The storm parameters DstMin, $(dDst/dt)_{MPmax}$, AE_{max}, Kp_{max}, $\langle AE_{MP} \rangle$, and $\langle Kp_{MP} \rangle$ can identify only 1 or 2 of the SvSW events. Using an IpsDst threshold of -250 nT in Kyoto Dst, we demonstrate a 100% true SvSW identification rate with only one false NSW.

4. The lone SvSW event occurred during a non-super storm on 1972 August 04 that appears low impulsive in Dst data (has a low value of IpsDst) is identified as a false NSW. Actually, it is also highly impulsive as revealed by the large H ranges (420 nT and 325 nT) of short durations (1 hour) observed in the available magnetograms at two Dst stations. The results indicate that it may be useful to consider high resolution IpsDst in the future.

5. The mechanism of large IpsDst is investigated using the solar wind velocity V and IMF Bz measured by the ACE satellite since 1998. The mechanism involves the

coincidence of high ⟨V_{MP}⟩ containing a high ICME front velocity △V (sudden increase by over 275 km s^{-1}) and large ⟨Bz_{MP}⟩ southward covering △V. Their combined impulsive action can cause impulsive entry of a large amount of high-energy charged particles into the magnetosphere and ring current through continuous and rapid magnetic reconnection leading to large IpsDst and SvSW, through impulsive solar wind-magnetosphere-ionosphere-ground system coupling.

Acknowledgments

We thank the referee of this paper for the critical comments and helpful suggestions that have improved the quality of the paper. He/she deserves to be a co-author. We also thank M. Nose and T. Iyemori of Kyoto University (WDC) for the scientific discussions and magnetograms on 1972 August 04-05 recorded at the Dst observatories at Kakioka, San Junn, Honolulu, and Hermanus which are available at http://www.kakioka-jma.go.jp/en/index.html, https://geomag.usgs.gov/ and http://www.sansa.org.za/spacescience, respectively. We acknowledge the use of Kyoto Dst and USGS Dst data available at http://swclob-kugi.kyoto-u.ac.jp and http://geomag.usgs.gov/data), and SymH index available at http://wdc.kugi.kyoto-u.ac.jp/aeasy. This research was supported by the National Key R&D Program of China (2018YFC140730， 2018YFC1407303), the National Natural Science Foundation of China (grants 41604139, 41574138, 41774166, 41431072, 41831072), the Chinese Meridian Project, the foundation of National Key Laboratory of Electromagnetic Environment (grants 6142403180102, 6142403180103), and JSPS KAKENHI (15H05815 and 16H06286) in Japan. Work at Los Alamos was performed under the auspices of the U.S. Department of Energy with support from the NASA-ACE program.

References

Albertson, V. D. & Thorson, J. M. 1974 IEEE Trans Power App&Sys **PAS-93** 1025

Albertson, V. D., Thorson,J. M. & Miske, S. A. 1974 IEEE Trans Power App&Sys **PAS-93** 1031

Anderson, C.W., Lanzerotti, L. J. & Maclennan, C. G. 1974 BellSys Tech J **53** 1817

Aran, A., Sanahuja, B., & Lario, D. 2005 AnnGeophys **23** doi:10.5194/angeo-23-3047-2005.

Baker, D. N. et al. 2008 1-144 The National Academy Press, Washington, DC, 1-144

Balan, N., Skoug, R., TulasiRam, S., Rajesh, P. K., Shiokawa, K., Otsuka, Y., Batista, I. S., Ebihara Y., & Nakamura T. 2014 JGR **119** doi:10.1002/2014JA020151

Balan, N., Batista, I. S., TulasiRam, S. & Rajesh, P. K. 2016 Geoscience Letters **3.3** doi:10.1186/s40562-016-0036-5

Balan, N., Ebihara, Y., Skoug, R., Shiokawa, K., Batista, I. S., TulasiRam, S., Omura, Y., Nakamura, T., & Fok, M.-C. 2017a. JGR **122***,* doi:10.1002/2016JA023853

Balan, N., TulasiRam, S., Kamide, Y., Batista, I. S., Souza, J. R., Shiokawa, K., Rajesh, P. K., & Victor, N. J. 2017b EPS, **69:59**, doi10.1186/s40623-017-0642-2

Boteler, D. H. 2001 AGU Geophysical Monograph **125** 347-352

Boteler, D.H., & Beek, G. J. 1999 GeoRL **26** 577

Borovsky, J. E., Hesse, M., Birn, J., & Kuzentsova, M. M. 2008 JGR **113** A07210

Burlage, L., Sittler, E., Mariani, F., & Schwenn, R. 1981 JGR **86** 6673-6684

Burton, R. K., McPherron, R. L., & Russell, C. T. 1975 JGR **80** 4204

Carrington, R. C. 1859 Mon. Not. R. Astron. Soc. **20** 13

Cid. C., Palacios, J., Saiz, E., Guerrero, A., & Cerrato, Y. 2014 JSWSC **4** A28 doi:10.1051/swsc/2014026

Cliver, E. W., Feynman, J., & Garrett, H. B. 1990 JGR **95** 17103

Cliver, E. W., & Svalgaard, L. 2004 *SoPh* **224** 407

Cliver, E. W., & Dietrich, W. F. 2013 **3** A31, doi:10.1051/swsc/2013053.

Davidson, W.F. 1940 Edison Electric Institute Bulletin July.

Eastwood, J. P., et al. 2017 Risk Analysis **37** *(2)* 206

Ebihara, Y., et al. 2005 JGR **110**, A09S22

Fok, M.-C., Wolf, R. A., Spiro, R. W., & Moore, T. E. 2001 JGR **106** 8417

Gonzalez, W. D, Joselyn, J. A., Kamide, Y., Kroehl, H. W., Rostoker, G., Tsurutani, T. B., & Vasyliunas, V. M. 1994 JGR*,* **99**, 5771

Gopalswamy, N., Yashiro, S., Michalek, G., Xie, H., Lepping, R. P., & Howard, R. A. 2005 GeoRL doi:10.1029/2004GL021639

Green, J. C., Likar, J. & Shprits, Y. 2017 SpWea **15** 804

Iyemori, T., Araki, T., Kamei, T., & Takeda, M. 1992 No**. 1** 1989, Data Anal. Center for Geomagn. and Space Magn., Kyoto Univ., Japan.

Hapgood, M. A. 2011 AdSpR **47**, 2059

Kamide, K., & Balan, N. 2016 Geoscience Letters **3:10** https://doi.org/10.1186/s40562-016-0042-7.

Kappenman, J., G. 2003 SpWea **1** NO. 3, 1016

Kappenman, J. G. 2006 AdSpR **38(2)** doi.org/10.1016/j.asr.2005.08.055.

Klimas, A. J., Vassiliadis, D., & Baker, D. N. 1997 JGR **102** 26993

Kohavi, R., & Provost, F. 1998 On Applied Research in Machine Learning **30** Columbia University New York

Lanzerotti, L. J. 1983 SSRv **34** 347

Lanzerotti, L., J. 1992 Geo. Physics. Res. **19** 19

Liemohn M. W., Jazowski, M., Kozyra, J. U., Ganushkina, N., Thomsen, M. F., & Borovsky, J. E. 2010 *Proc. R. Soc. A* **466** *3305*

Love, J. J., & Gannon, J. L. 2009 AnGeo **28(8)** 3101

Love, J. J., Rigler, E. J., Pulkkinen, A., & Riley, P. 2015 *GeoRL* **42** 6544

Love, J. J., & Coïsson, P. 2016 1941 Eos **97** doi:10.1029/2016EO059319

Love, J. J., Lucas, G. M., Kelbert, A., & Bedrosian, P. A. 2017 GeoRL doi: 10.1002/2017GL076042

Love, J. J. 2018, SpWea, **16** doi.org/10.1002/2017SW001795.

Lühr, H., Xiong, C., Olsen, N., & Le, G. 2017 SSRv **206** 521–545

Marshall, R. A., Dalzell, M., Waters, C. L., Goldthorpe, P., & Smith, E. A. 2012 SpWea **10** S08003, doi:10.1029/2012SW000806

Mayaud, P. N. 1972 JGR **77** 6870-6874

McComas, D. J., Bame, S. J., Barker, P., Feldman, W. C., Phillips, J. L., & Riley, P. 1998 *SSRv* **86** 563

Medford et al. 1989 *GoRL **16**(10)* 1145

Nagatsuma, T., Kataoka, R., & Kunitake, M. 2015 EPS **67:78** doi:10.1186/s40623-015-0249-4.

Newell, P. T., Sotirelis, T., Liou, K., Meng, C.-I., & Rich, F. J. 2007 JGR **112** A01206 doi:10.1029/2006JA012015

Pulkkinen, T. 2007 Living Rev Solar Phys **4** 1

Pulkkinen, A., Lindahl, S., Viljanen, A., & Pirjola, R. 2005 SpWea **3** S08C03 doi:10.1029/2004SW000123

Ribeiro, P., Vaquero, J. M., Gallego, M. C., & Trigo, R. M. 2016 SpWea **14** doi:10.1002/2016SW001424.

Rostoker, G., Samson, J. C., Creutzberg, F., Hughes, T. J., McDiarmid., D. R., McNamara, A. G., Vallance Jones, A., Walls, D. D., & Cogger, L. L. 1995 SSRv **46** 743

Schrijver, C. J., et al. 2015 AdSpR ***55*****(12)** 2745

Singh, A. K., Devendra Singh, & Singh, R. P. 2010 SurvGeophys **31** 581

Skoug, R. M., Gosling, J. T., Steinberg, J. T., McComas, D. J., Smith, C. W., Ness, N. F., Hu, Q., & Burlaga, L. F. 2004 JGR **109** A09102

Slothower, J.C., & Albertson, V. D. 1967 J Minn Academy Science **34** 94

Smith, E. J., & Wolfe, J. H.1976 Geo Physics Res **3** 137

Sugiura, M. 1964 Ann. Int. Geophysical Year*,* **35** 9-45 Pergamon New York

Sugiura, M., & Kamei, T. 1991 IAGA Bull. **40***,* Int Serv of Geomagn Indices Saint-Maur-des-Fosses France

Svalgaard L. 1977 edited by J. B. Zirker 371–441 Colo Assoc Univ Press Boulder

Tsurutani, B. T., Gonzaez, W. D., Tang, F., Lee, Y. T., Okada, M., & Park, D. 1992 GoRL **19** 1993

Tsurutani, B. T., Gonzalez, W. D., Lakhina, G. S., & Alex, S. 2003 JGR **108** 1268

Vaisberg, O.L., & Zastenker, G. N. 1976 SSRv **19** 687

Viljanen, A., Koistinen, A., Pajunpää, K., Pirjola, R., Posio P., & Pulkkinen, T. 2010 Geophysica **46** 59

Viljanen, A., Pirjola, R., Pracser, E., Ahmadzai, S., & Sing, V. 2013 SpWea **11** 575

Witasse et al. 2017 JGR **122** 7865

Wik, M., Pirjola, R., Lundstedt, H., Viljanen, A., Wintoft, P., & Pulkkinen, A. 2009 AnGeo **27** 1775

Zhang, R., Liu, L., Le, H., Chen, Y., & Kuai, J. 2017 JGR **122**. https://doi.org/10.1002/2017JA024637

Zhu., D., Billings, S. A., Balikhin, M. A., Wing, S., & Alleyne, H. 2007 JGR **112** A06205

Table and Figure captions

Table 1. Table lists the storm numbers and dates of IpsDst in Figure 6a and corresponding other parameters including SvSW/NSW. The values of the other parameters in Figure 6 do not correspond to the same number and date because of their increasing or decreasing ordering.

Table 2: The truth table lists the number of (a) true SvSW, (b) false SvSW, (c) true NSW, and (d) false NSW events identified by IpsDst for a threshold of -250 nT in Kyoto Dst.

Figure 1. Scatter plot of hourly Kyoto Dst against USGS Dst in 1958-2007.

Figure 2. Comparison of four super storms (DstMin ≤-250 nT) in Kyoto Dst (blue) and USGS Dst (red) having large IpsDst (purple shade) and comparatively weak IpsDst (yellow shade). MPOs are identified by a computer program satisfying storm selection criteria and IMF Bz turning southward. The time T0 of X-axis corresponds to 12 UT on 2003 October 28 (panel a), 2001 November 05 (panel b), and 2003 November 19 (panel c), respectively.

Figure 3. An example identifying the storm main phase MP in Dst, Kp, and AE storms.

Figure 4. Scatter plot of the absolute and percentage differences (Kyoto minus USGS) in DstMin (a and b) and IpsDst (c and d) of the storms in the two Dst indices as function of time, with red color for super storms and blue color for intense and moderate storms together. The average differences are noted inside brackets.

Figure 5. Scatter plot of IpsDst against DstMin of the Carrington storm and all common storms during 1958-2007 in (a) Kyoto Dst and (b) USGS Dst. Red and green dots correspond to SvSW events. Regions 1-2 and 2-3 represent the IpsDst ranges of NSW and SvSW events including the uncertainty in IpsDst due to the uncertainty in T_{MP} of the respective highest and lowest

IpsDst values. The horizontal bars show the uncertainty in IpsDst of the SvSW events only for simplicity and limited to ±100 nT for the Carrington event.

Figure 6. IpsDst, T_{MP}, DstMin, $(dDst/dt)_{MPmax}$, and F10.7 on the days of DstMin of the super storms (DstMin ≤-250 nT) in Kyoto Dst arranged in their increasing or decreasing orders. The Carrington storm of 1859 and intense storm on 1972 August 04 are included. Red color corresponds to SvSW and blue color to NSW (see text).

Figure 7. IpsDst, T_{MP}, DstMin, $(dDst/dt)_{MPmax}$, and F10.7 on the days of DstMin of the super storms (DstMin ≤-250 nT) in USGS Dst arranged in increasing or decreasing orders of the parameters. The Carrington storm of 1859 and intense storm on 1972 August 04 are included. Green color corresponds to SvSW and black color to NSW (see text).

Figure 8. $\langle Kp_{MP} \rangle$, Kp_{max}, $\langle AE_{MP} \rangle x10^{-2}$, and $AE_{max}x10^{-2}$ arranged in their decreasing orders. The parameters correspond to the Dst storms shown in Figure 6a. The Carrington event has no Kp data and five events including the Carrington and 1972 August 04 events have no AE data. Red and blue colors correspond to SvSW and NSW, respectively.

Figure 9. Scaled values (5-minute resolution) of the H component magnetograms on 1972 August 04-05 at the Dst stations (a) Kakioka and (b) San Juan with standard deviations; zero corresponds to baseline levels of 30094 nT and 27440 nT, respectively. The corresponding (c) hourly H values at all four Dst stations used for computing the (d) Dst index are shown. Important parameter values are listed.

Figure 10. IpsDst of the super Dst storms (Kyoto Dst) since 1998, Carrington storm (number 1), and 1972 August storm (number 15) and corresponding $\langle V_{MP} \rangle x \langle Bz_{MP} \rangle$, $\langle V_{MP} \rangle$, $\langle Bz_{MP} \rangle$, △V, and $Bz_{\triangle V}$ obtained from ACE data and adopted from theoretical values available in the literature (see text). All parameters are arranged in increasing order of IpsDst with red color for SvSW.